MOLECULAR PHYSICS, 1996, VOL. 89, NO. 5, 1373–1396

Far-infrared VRT spectroscopy of two water trimer isotopomers: vibrationally averaged structures and rearrangement dynamics

By K. LIU, M. G. BROWN, M. R. VIANT, J. D. CRUZAN and R. J. SAYKALLY

Department of Chemistry, University of California, Berkeley, CA 94720, USA

(*Received 5 January 1996; accepted 28 June 1996*)

We report the measurement of far-infrared vibration–rotation tunnelling parallel bands of two partially deuterated water trimer isotopomers: $(D_2O)_2DOH$ and $(H_2O)_2DOH$ at 97·2607 cm^{-1} and $\sim$ 86 cm^{-1}, respectively. The hydrogen bond rearrangement dynamics of the two mixed trimers can be described by the simplified molecular symmetry G_8, which accounts for both the flipping and bifurcation tunnelling motions previously established for $(H_2O)_3$ and $(D_2O)_3$. The observed donor tunnelling quartet, rather than triplet, splitting indicates that the two homogeneous monomers (D_2O or H_2O) in each mixed trimer experience slightly different environments. Vibrationally averaged structures of $(H_2O)_3$, $(D_2O)_3$, and $(D_2O)_2DOH$ were examined in a Monte Carlo simulation of the out-of-plane flipping motions of the free atoms. The simulation addresses both the symmetric top behaviour and the negative zero-point inertial defect for $(H_2O)_3$ and $(D_2O)_3$, which were insufficiently counted in all previous structure models. The average ground state O—O separations, which are correlated to other angular coordinates, were determined to be 2·84 $\pm$ 0·01 Å for all three species. The simulated difference in hydrogen bond nonlinearity also supports the inequivalency of the two homogeneous monomers. The structural simulation shows that the unique H in $(D_2O)_2DOH$ is free, while a torsional analysis suggests the unique D in $(H_2O)_2DOH$ is bound within the cyclic ring. Both bands can be assigned to the pseudorotational transitions which correlate to those found in the pure trimers.

1. Introduction

The subject of structure and hydrogen bond rearrangement dynamics of water clusters in general [1–23] and the water trimer in particular [6, 9–11] has attracted considerable recent attention [24–42]. Spectroscopic efforts on this subject are motivated largely by the continued quest for an accurate characterization of the pairwise and many-body intermolecular interactions that are fundamental to the description of the condensed phases of water [20, 43–51]. While characterization of cluster structures clearly provides a fundamental probe of the corresponding intermolecular potential energy surface (IPS), it is the measurement of the dynamics, the intermolecular vibrations and associated tunnelling splittings that result from hydrogen bond network rearrangements (HBNR), that calibrates our understanding of the details of molecular interactions [52].

Recent far-infrared (FIR) vibration–rotation tunnelling (VRT) spectroscopic studies of $(H_2O)_3$ and $(D_2O)_3$ [9–11] have revealed that (1) the asymmetric global minimum energy structure of the cyclic trimer is averaged over the 'flipping' dynamics (low barrier motion) to become a symmetric oblate rotor on the time scale of overall rotations, (2) the quartet tunnelling fine structure pattern associated with each rovibrational transition arises from a higher barrier pathway called 'donor tunnelling'

or 'bifurcation' [31], and (3) the appropriate molecular symmetry group describing both of these hydrogen tunnelling motions is G_{48}. These findings agree well with previous *ab initio* theories [13, 18, 19, 25, 28, 29, 32, 33] and were supported subsequently by a series of dynamics calculations by Leutwyler and co-workers [19, 34–39, 53, 54], wherein the observed FIR vibrations were assigned to a manifold of pseudorotational states caused by the flipping motions. Approximate calculations of the tunnelling splittings in the pure trimers have been carried out by Wales [30], treating tunnelling matrix elements analogous to the Hückel resonance integrals in conjugated π electron systems, and by Gregory and Clary using the diffusion quantum Monte Carlo (DQMC) method [40, 41], who also demonstrated that non-pairwise additive three-body forces are important in determining the trimer structure. This is in agreement with the *ab initio* calculations by Xantheas and others, which predict that three-body interactions contribute at least 10% of the total binding energy [27] in the water trimer.

Despite the extensive theoretical and experimental work on the structure and VRT dynamics of the $(H_2O)_3$ and $(D_2O)_3$, there has been little effort to address the isotopically mixed trimers. Measurements of the mixed trimers provide complementary tests of the IPS. Having lower symmetry and exploring diverse regions of

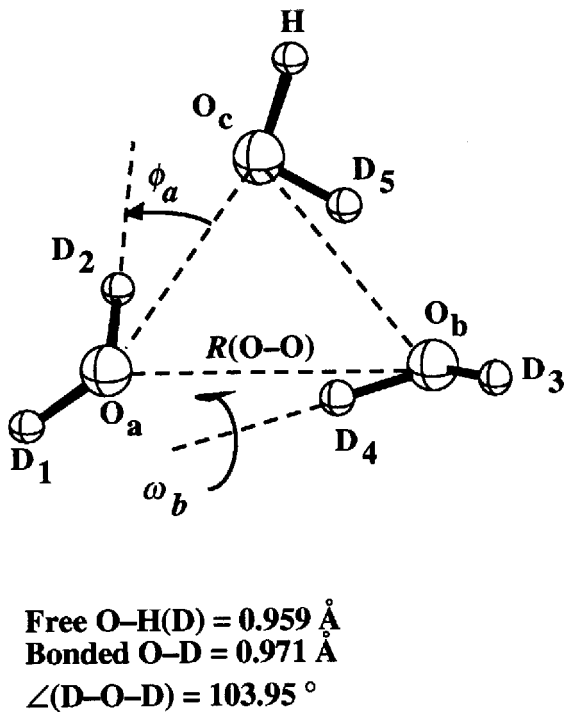

Figure 1. Structure of the trimer-d_5 and the definitions of the intermolecular coordinates. $R(\,)$: the inter-oxygen distance. ϕ_i with $i = a, b, c$: the in-plane angle between the bonded O_i—D and $O_i \cdots O_j$, where O_i—D is D bonded to O_j; ϕ_a is designated to characterize the nonlinearity of the O_a—D$\cdots O_c$ bond, similarly ϕ_b and O_b—D$\cdots O_a$ bond and ϕ_c the O_c—D$\cdots O_b$ bond. ω_i with $i = a, b, c$: the monomer torsional (flipping) angle about its bound O–D bond; $\omega_i = 0$ corresponds to the free O–D(H) bond in the O—O—O plane. The ω_i angles were sampled in the simulation according to the double Gaussian pdf shown in figure 5.

the IPS, the mixed isotopic species may exhibit different VRT dynamics and different vibrationally averaged structures from those found in the homogeneous trimers. It is the purpose of this initial study of the mixed trimers to quantify these differences. Moreover, the symmetry-breaking control of the HBNR tunnelling that is achieved through isotope substitution in the trimer can lend insights into the tunnelling behaviour in the larger clusters, wherein the dynamics can be simplified by the constraining hydrogen bonding network, as found in the recent study of the cage form of $(H_2O)_6$ [55].

In this paper, we report the measurements of a VRT band of a penta-deuterated water trimer, referred to hereafter as the trimer-d_5, together with a mono-deuterated trimer band (trimer-d_1), and also characterization of the associated HBNR dynamics pertinent to other mixed trimers. In an attempt to improve previous model structural parameters (figure 1), we employ a Monte Carlo (MC) simulation of the large amplitude out-of-plane flipping motions of the free O–H(D) bonds to determine the vibrationally averaged structures of $(H_2O)_3$, $(D_2O)_3$, and $(D_2O)_2DOH$. The two essential structural features, exact oblate top behaviour (Ray's asymmetry parameter $\kappa = 1$) of the homogeneous trimers and non-planarity (zero-point inertial defect $\Delta_0 < 0$), were both reproduced in the simulation.

2. Experimental

The Berkeley tunable FIR laser spectrometer used in this work has been described previously [56]. Briefly, mixing tunable microwave radiation (ν_{mw}) and the FIR (ν_{FIR}) laser on a Schottky barrier diode generates tunable FIR sidebands ($\nu_{sb} = \nu_{FIR} \pm \nu_{mw}$). Direct absorption measurements were carried out by monitoring the sideband power with a Ge:Ga photoconductor. Water clusters were produced in a planar supersonic expansion of Ar bubbled through ambient temperature water into a chamber evacuated by a 1200 $ft^3\,min^{-1}$ Roots pump, using a newly designed pulsed slit (102•3 mm × 0•125 mm) valve [57]. To verify that the signals observed originated from pure water clusters, other carrier gases such as He and Ne (70% in He) were also used. Intersecting the supersonic jet with 22 passes between a pair of confocal mirrors, the laser sidebands were frequency modulated and recovered at $2f$ ($\sim$ 100 kHz) detection by a lock-in amplifier with a time constant of 100 μs. The transient (1•2 ms FWHM) signal from the lock-in was fed into two boxcar integrators, one sampled the peak, the other the baseline, and the difference of the two was displayed as a function of frequency on a PC 486. Limited by the Doppler broadening that results from the non-orthogonal intersection of the laser beam and the supersonic jet, the typical linewidth is $\sim$ 5 MHz at 100 cm^{-1}. The precision of the line position is $\pm$3 MHz due to the FIR laser frequency drift. The use of the pulsed [57], instead of the previous CW planar expansion [58], has enabled us not only to achieve an order of magnitude increase in signal-to-noise ratio on previously observed cluster absorptions, but also to detect the less abundant species, such as the trimer-d_5, even with a 99•9% D_2O solution, wherein the probability of forming $(D_2O)_3$ is 999 times greater.

The spectroscopic determination of the cluster size was facilitated by an isotope mixture test. For a pure water cluster, a specific VRT transition intensity is proportional to (monomer mole fraction)^n or equivalently, $(f_{H,D})^{2n}$, where n is the cluster size and $f_{H,D}$ is the atomic mole fraction of H or D. A logarithmic plot of the line intensity versus $f_{H,D}$ yields a straight line with the slope equal to twice the cluster size. Affecting mainly the intercept of the straight line, the isotope dependence of the

mole fraction would not be critical here for establishing the cluster size. For a mixed water cluster, the above relation is modified as follows:

$$\text{Absorption intensity} \propto (f_H)^{N_h}(1-f_H)^{N_d}, \quad (1)$$

where N_h and N_d are the numbers of protons and deuterons in the mixed cluster, respectively, $N = N_h + N_d$ is twice the size of the cluster, and $f_D = 1 - f_H$. The first factor is derived from the proton contribution, the second from the deuteron. A plot of spectral intensity versus f_H can yield N_h, assuming $N = 4$, 6, etc., for the dimer, trimer, respectively. Since there are two parameters, N_h and N in equation (1), a second constraint, that N_h has to be an integer within the standard deviation (SD), is necessary to determine N unambiguously. A convenient generalization from equation (1) is that a specific isotopomer signal intensity can be optimized at a H:D mole fraction of $N_h:N_d$. Therefore, an $\sim 84\%$ D_2O (close to the optimal 1:5 H:D ratio) solution was used for the trimer-d_5 scanning, and $\sim 84\%$ H_2O for the $-d_1$ isotopomer. Only two parameters, N_h and N_d or their equivalents such as the overall size, can be uniquely determined experimentally because there exist only two constraints. The actual hydrogen bonding pattern has to be established through analyses of the rotational constants and the tunnelling splittings that act as a fingerprint for each isotopic species, e.g., for a given mixed trimer with $N = 6$ and $N_h = 2$, one cannot distinguish $(HOD)_2D_2O$ from $H_2O(D_2O)_2$ by the isotope test alone, whereas the spectral patterns are quite distinct.

For the trimer-d_5 signal, a log (intensity) versus f_H plot was measured at $f_H = 16\%$, 25%, and 50% and fitted using equation (1) with $N = 6$ (trimer) (figure 2). The resulting N_h was $1{\cdot}130 \pm 0{\cdot}134$ at a 95% confidence level, while with N fixed at other even numbers, a non-integral N_h was obtained, e.g., with $N = 4$ we had $N_h = 0{\cdot}585 \pm 0{\cdot}001$. Qualitatively, the signal intensity was found to be optimized at $f_H = 16\%$, a H:D ratio close to 1:5. We concluded, therefore, that the absorption was due to a water trimer.

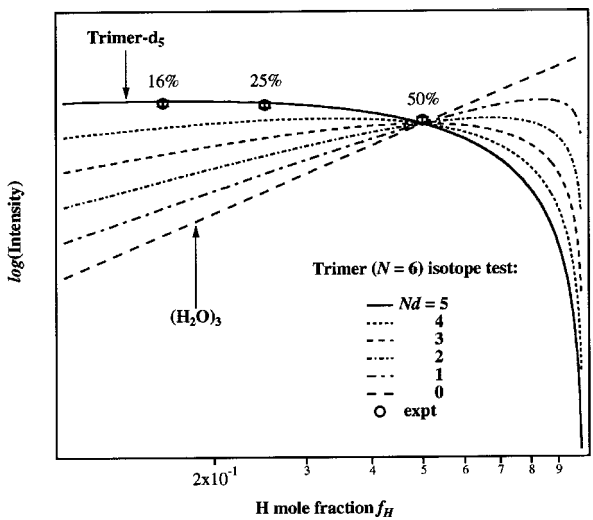

Figure 2. Log (intensity) versus f_H used to initially identify the mixed trimer according to equation (1). The f_H axis is in a logarithmic scale. Three experimental data points at $f_H = 16\%$, 25%, 50% quantitatively fit best with the trimer-d_5 curve, and qualitatively agree with expected behaviour: optimal signal at 16%.

3. Results

Each rovibrational transition of the trimer-d_5 was identified by its distinctive tunnelling fine structure pattern, as well as by a preliminary isotope test. As shown in the insets of figure 3, the intensity ratios of the $K_c \neq 0$ quartet components are 4:2:2:1, and the spacings among them are 10•5, 3•2, and 10•5 MHz, respectively. For all the $K_c = 0$ states, only a triplet with an intensity ratio of 4:4:1 was observed with equal spacings of 8•3 ± 0•3 MHz.

An extensive parallel c-type ($\Delta K_c = 0$) VRT band of the trimer-d_5 was recorded at 97•2607 cm^{-1}, the experimental stick spectrum of which is displayed in figure 3

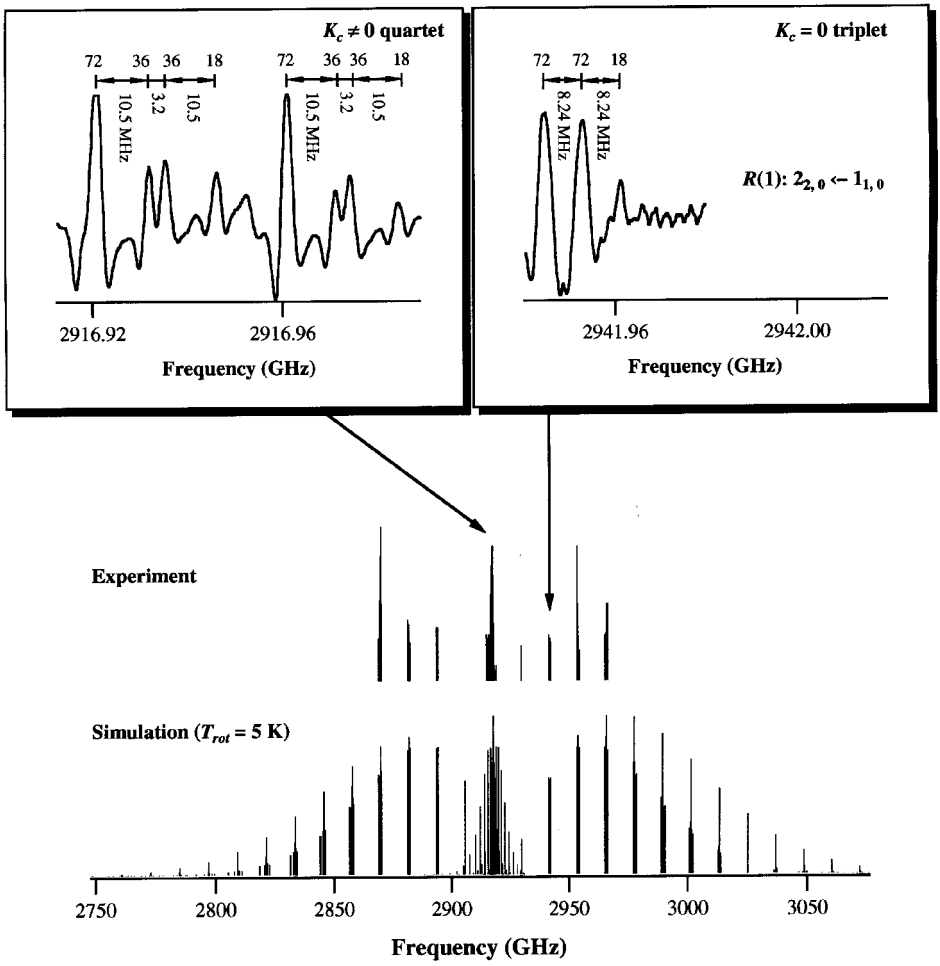

VRT Spectra of the Trimer-d_5 (free H)

Figure 3. Experimental and simulated stick spectra of the c type trimer-d_5 band at 97•26 cm^{-1}. The insets show the actual tunnelling pattern associated with each rovibrational transition, namely, quartets and triplets for the $K_c \neq 0$ and $K_c = 0$ states, respectively. Second derivative lineshapes are displayed. Also labelled above each peak are the nuclear spin weights.

Table 1. Assigned trimer-d_5 transitions. Only the A_a component transition frequencies are listed.

J'	K'_a	K'_c	←	J''	K''_a	K''_c	Obs./MHz	Obs. − Calc./MHz[a]
2	1	1		1	0	1	2941428·0	1·5
2	2	1		1	1	1	2942191·0	1·5
3	2	1		2	1	1	2953220·2	1·5
3	1	2		2	0	2	2953625·8	− 12·7
3	2	2		2	1	2	2953774·0	0·7
3	3	1		2	2	1	2954344·7	− 1·6
4	3	1		3	2	1	2965042·7	4·8
4	2	3		3	1	3	2965653·3	− 5·9
4	3	2		3	2	2	2965717·8	− 7·9
4	4	1		3	3	1	2966474·2	3·0
1	0	1		2	1	1	2894095·3	0·7
1	1	1		2	2	1	2893388·5	0·5
2	1	1		3	2	1	2882163·8	0·6
2	0	2		3	1	2	2881804·2	0·6
2	1	2		3	2	2	2881676·2	− 1·9
2	2	1		3	3	1	2881117·7	− 1·2
3	2	1		4	3	1	2870192·8	4·7
3	1	2		4	2	2	2869844·0	− 6·8
3	0	3		4	1	3	2869668·0	− 4·5
3	1	3		4	2	3	2869657·8	− 3·9
3	2	2		4	3	2	2869544·9	− 3·5
3	3	1		4	4	1	2868797·3	1·4
3	1	3		3	0	3	2917714·9	2·3
3	0	3		3	1	3	2917711·0	2·2
4	1	4		4	0	4	2917646·3	2·5
5	1	5		5	0	5	2917564·1	2·7
6	1	6		6	0	6	2917466·5	2·5
7	1	7		7	0	7	2917354·0	2·7
8	1	8		8	0	8	2917224·1	0·7
9	1	9		9	0	9	2917080·2	0·1
10	1	10		10	0	10	2916920·8	− 0·3
11	1	11		11	0	11	2916746·2	− 0·2
12	1	12		12	0	12	2916555·1	− 0·4
13	1	13		13	0	13	2916346·9	− 1·1
2	0	2		2	1	2	2917729·7	0·9
2	1	2		2	0	2	2917799·8	3·7
3	2	2		3	1	2	2917849·7	1·7
4	3	2		4	2	2	2918058·2	2·2
1	1	1		1	0	1	2918173·9	3·7
2	2	1		2	1	1	2918857·1	2·7
6	4	3		6	3	3	2917503·5	− 7·6
4	2	2		4	3	2	2917119·7	2·6
6	3	4		6	2	4	2917391·4	− 0·6
1	0	1		1	1	1	2917432·1	2·4
7	4	4		7	3	4	2917263·0	− 3·6
9	2	8		9	1	8	2917030·5	− 5·3
7	4	3		7	5	3	2916961·1	2·3
10	3	8		10	2	8	2916858·1	4·5
11	5	6		11	6	6	2916766·6	1·3
8	5	3		8	6	3	2916593·0	1·4
5	3	2		5	4	2	2916461·2	5·0
12	5	8		12	4	8	2916548·3	0·6

Table 1. *Continued.*

J'	K'_a	K'_c	←	J''	K''_a	K''_c	Obs./MHz	Obs. − Calc./ MHz[a]
13	5	9		13	4	9	2916380·8	2·6
13	4	10		13	3	10	2916341·6	− 0·3
9	6	3		9	7	3	2916122·6	− 9·4
10	7	3		10	8	3	2915594·1	3·4
1	1	0		0	0	0	2929618·4	*
2	2	0		1	1	0	2941994·2	*
3	3	0		2	2	0	2953880·9	*
1	1	0		2	2	0	2893494·2	*
2	2	0		3	3	0	2881632·2	*
3	3	0		4	4	0	2869544·9	*

Ground state combination differences

J''	K''_a	K''_c	←	J''	K''_a	K''_c	Obs./MHz	Obs. − Calc./ MHz
2	2	0		0	0	0	36124·2	2·1
3	3	0		1	1	0	60312·0	3·9
4	4	0		2	2	2	84645·3	1·1

[a] Asterisk signifies assigned by combination differences.

together with the simulation. The vibrationally averaged structure of the trimer-d_5 is a near-oblate top with resolvable asymmetry doubling. Due to the lack of prior molecular constants, the spectral assignment was established by iterative comparisons between the observed transitions and those predicted from the molecular parameters in the trial fits. The final assignment was confirmed by successfully measuring additional predicted lines. Finally, the line positions of the strongest component of each quartet were fitted using a Watson S-reduced Hamiltonian. The assigned lines and resulting spectroscopic constants from the least-squares fit are summarized in tables 1 and 2, respectively.

The VRT spectrum of the trimer-d_5 was found to be slightly perturbed. This is indicated by the necessary use of the d_1 distortion constant for the excited state to ensure a good fit. The spectral perturbation is also evident in all the transitions involving $K_c = 0$, which were not included in the fit. The assignment of these lines was made possible by using the ground state combination differences (table 1). It was observed that all the $K_c = 0$ multiplets were triplets; the middle doublet spaced by 3·2 MHz in the corresponding $K_c \neq 0$ quartets have merged into a broad singlet, resulting in an intensity pattern of 4:4:1. Ascribing this anomaly to a Coriolis mixing between the overall rotation and the flipping motion is consistent with the permutation-inversion (PI) group theoretical analysis that follows.

A c-type band of the trimer-d_1 near ~ 86 cm^{-1} was also observed but not assigned completely. The quartet VRT pattern has been identified again with an intensity ratio close to 9:3:3:1 and the respective spacings are 265, 12·5, and 265 MHz: much larger than those found in the trimer-d_5.

The equilibrium structure of the trimer has been shown in numerous high level calculations to be a hydrogen bonded cyclic ring with the unbound hydrogens above

Table 2. Spectroscopic constants of the trimer-d_5 c type band (in MHz). The rms of the fit is 3·77 MHz. The 2σ uncertainties in the last digits are listed in the parentheses.

Ground state	
A''	6195·69(29)
B''	5833·90(25)
C''	Arbitrarily fixed[a]
D''_{JK}	0·13497 (fixed)[b]
Excited state	
A'	6192·48(28)
B'	5811·80(29)
$C'-C''$	−7·871(51)
D'_{JK}	0·13584(33)
d'_1	−0·2398(16)
Band origin ν_0	2917820·44(87)

[a] The C constants cannot be determined in a parallel band.

[b] D''_{JK} and D'_{JK} were correlated if varied in the fit.

and below the O···O···O plane [13, 18, 19, 28, 29, 34]. From the measured rotational constants of the trimer-d_5, we are able to determine that the unique H atom is in an unbound position, using a Monte Carlo simulation of the trimer structure averaged over the large amplitude flipping motions. Additional support for this conclusion comes from the vibrational analysis presented below. The unique D in the trimer-d_1, however, is rationalized as being bound, on the basis of an effective 3-dimensional torsional Hamiltonian.

4. Tunnelling pattern analysis

In analysing the tunnelling fine structure associated with each rovibrational transition, we employed PI group theory, which is useful for classifying the symmetries of the VRT states supported by degenerate structures. The eigenstate splittings arise only from the degenerate feasible tunnelling among minima corresponding to symmetrically equivalent frameworks; tunnelling between non-degenerate or inequivalent frameworks can change only the magnitudes of the existing splittings, and therefore is not necessary for a calculation of the tunnelling patterns by the spin weight ratios. Finally, the number of connectable frameworks is equal to the size of the appropriate PI group, and one should practically use the simplest possible group, the molecular symmetry (MS) group, to rationalize the *resolvable* splittings.

For a pure water trimer isotopomer, there exist 96 equivalent minima on the 12-dimensional IPS. Two feasible tunnelling motions, called 'flipping' and 'donor tunnelling' in our previous work [9], have been identified within two disjoint subsets of 48 frameworks each, and the appropriate MS group is G_{48}; a connection between the two subsets exists via a third high-barrier motion referred to as 'cw-ccw' tunnelling in the work by Pugliano and Saykally and later found unfeasible. Experimentally, this was established by comparing the measured intensity ratios of the quartet components in the VRT spectra with the statistical nuclear spin weights predicted from the appropriate MS group. Assumptions of a different tunnelling pathway can lead to

qualitatively different spectral patterns. Specifically, the zero spin weights found for $K_c \neq 3n$ states of $A_2^{\pm}$ or $A_3^{\pm}$ symmetry corresponding to the missing transitions in the $(H_2O)_3$ spectrum allowed us to determine unmistakably the size of the MS group as G_{48}. Theoretical studies can yield identical results by examining the detailed tunnelling dynamics on *ab initio* IPS [30, 31, 34, 40].

In the isotopically mixed trimers, the number of structurally equivalent minima is greatly reduced. For the trimer-d_5, the largest possible PI group is G_{16}, considering the permutations ($(2!)^2$) of the deuterons within two identical monomers and monomers themselves (2!), and the space fixed inversion E*. Since permutation of the two identical monomers would correspond to the unfeasible cw-ccw motion, the group is further reduced to G_8. The C_{3h} dynamic symmetry group of the flipping averaged homogeneous trimers is no longer a subgroup of G_8; in fact, the observation of asymmetry doubling in the VRT spectra establishes the absence of a 3-fold or higher symmetry axis in the trimer-d_5. In addition we note that (figure 1), because of the unique HOD monomer, the other two D_2O units are not equivalent in two senses. (i) Each D_2O monomer is in a different chemical environment relative to HOD: one is an acceptor and the other a donor; an analog of this difference can be recognized in the two forms of the distinct dimers, $HOD\cdots OD_2$ and $HDO\cdots DOD$ [59]. (ii) The configuration of the hydrogen bond between the two D_2O monomers becomes distinguishable: a *trans* configuration having the two unbound D atoms on the opposite sides of the bond is likely to be of lower energy than a *cis* geometry (this is in accord with the model of two types of hydrogen bond, 'strong' and 'weak', respectively, proposed for interpreting the recent high-resolution neutron scattering data on ice [60]). We now analyse the possible tunnelling dynamics in the trimer-d_5 based on the these considerations and the familiar homogeneous trimer tunnelling pathways.

First, the six inequivalent (equivalent for the homogeneous trimers) trimer-d_5 frameworks connected by successive single flips now resolve into 3 pairs of enantiomers. The E* operator converts each structure to its enantiomeric form. If E* is considered as a feasible degenerate tunnelling operator, this is equivalent to either the concerted flipping of all the unbound atoms or to two successive single flips by two different monomers [9]. The former has a planar transition state geometry of high potential energy (calculated 576 cm^{-1} above the global minimum, compared with the single flip transition state that is only 98 cm^{-1} [36, 37]), and the latter involves a long pathway. Both are expected to yield a tunnelling splitting much smaller than the rotational spacings, which have not been observed in our experiment. Allowing E* to be feasible in the trimer-d_5 would lead to a doublet pattern with symmetry labels A^+ and A^- (as the parity is $+1$ and -1, respectively) classified in the $C_s = \{E, E^*\}$ group. This does not reproduce the observed quartet feature, which includes two basic features, the unequal *spacings* and the *intensity* ratios.

However, since E* is commutable with the effective 3-dimensional torsional Hamiltonian [38, 39, 61] [also see equation (8) in section 6] derived for the flipping motions, the C_s group can be used to classify the torsional states, which are called the pseudorotational states for the three homogeneous species $(H_2O)_3$, $(D_2O)_3$ and $(HOD)_3$ with all the H or D atoms free. In the homogeneous trimers, the pseudorotational states can be classified under a cyclic group G_6, which is isomorphic with the PI group C_{3h}. The generator of G_6 is $F \equiv (abc)(153)(264)^* \equiv E^*(abc)(153)(264)$ [9] with a, b and c denoting the oxygen atoms (figure 1). Following the notations of van der Avoird *et al.* [61, 62], the irreducible representations (irreps) are labelled by

A_1^+, A_1^-, A_2^+, A_2^-, A_3^+, A_3^-, which have the complex characters $\exp(nm\pi i/3)$ for the operation F^n with the pseudorotational quantum number $m = 0, 3, -2, 1, 2, -1$, respectively. In the mixed trimers, pseudorotation is equivalent to an overall rotation of π about the principal c axis, as explained below. The cyclic permutation $F^* \equiv (abc)(153)(264)$ is no longer feasible. Therefore, the $A^\pm$ pseudorotational states classified under C_s relate to the irreps of G_6 as $A^\pm \leftrightarrow A_i^\pm$, $i = 1$, 2 and 3 (figure 4(*a*)). Note that degenerate states $\{A_2^-, A_3^-\}$ and $\{A_2^+, A_3^+\}$ become resolved in the mixed trimers due to the inequivalency of the three reduced flipping masses (section 6). Since the spacings between the pseudorotational states are much larger than the rotational energy separations, we can regard $A^\pm$ as the vibrational part of the symmetry of the VRT state; the $\Delta m = 1 \leftarrow 0$ spacings of $(D_2O)_3$ and $(H_2O)_3$ are $\sim 5\ cm^{-1}$ and $\sim 15\ cm^{-1}$ [38, 39], respectively, and the corresponding spacing of the mixed trimers are thus expected to lie in between, considering their reduced internal rotational constants.

Next, we consider the donor tunnelling pathway, an exchange motion analogous to the donor tunnelling ('bifurcation') in the water dimer. In the homogeneous trimer there are two possible rearrangements for such an exchange, as indicated by Wales [30]: the effective rotation of the monomer about its c axis (perpendicular to the monomer plane) accompanied by (i) either a single flip of the acceptor (relative to the exchanging monomer) (ii) or a double flip of both non-exchanging units. It was found in a study of the homogeneous water trimers by van der Avoird and co-workers [61, 62] that the donor tunnelling has to involve the inversion operator E*, which suggests exchange + double flip as the likely pathway. In the trimer-d_5, however, the exchange + single pathway no longer converts one framework to an equivalent form if one acknowledges the aforementioned differences between the two D_2O molecules. Again the exchange + double flip pathway accomplishes this. The generators for this tunnelling motion are (12)* and (34)* (table 3(*c*)) which belong to two different classes. We note that a third exchange motion, the effective pure rotation by π about the monomer C_2 axis, also constitutes a degenerate pathway. The operators for the effective C_2 tunnelling are (12) and (34) (table 3(*c*)). The actual C_2 motion may be a higher barrier or long path tunnelling process than the exchange + double flip pathway.

The fact that the two D_2O monomers are inequivalent forces the following donor tunnelling splitting pattern, which could be constructed in a stepwise (not required) manner. Allowing the more facile motion from a monomer experiencing the lower tunnelling barrier, say (12) or (12)*, introduces a doublet splitting of spacing β_1. A slightly higher barrier motion from the second monomer, (34) or (34)*, further splits each state into a doublet of smaller spacing β_2. A quartet pattern of spacings β_2, $(\beta_1 - \beta_2)$, β_2 resembling the observed *spacing* pattern is thus obtained. We must derive the state symmetry labels and their nuclear spin weights to establish the *intensity* pattern.

Combining the pseudorotation and donor tunnelling motions together results in a direct product PI group G_8. This is the largest possible MS group for the trimer-d_5 without considering the high-barrier cw-ccw tunnelling. The same symmetry group also applies to trimer-d_1 regardless of whether the unique D atom is abound or free. In order to calculate the nuclear spin weights and construct a tunnelling correlation diagram, one needs to satisfy the following relation: $\Gamma_{VRT} \otimes \Gamma_{nspin} \supset \Gamma_{int}$, where Γ_{VRT}, Γ_{nspin}, and Γ_{int} are the symmetry species of a VRT state, a nuclear spin state, and the complete internal wavefunction, respectively. The symmetry of the ground vibrational wavefunction is usually assumed to be totally symmetric, i.e., the irrep A_a^+ in G_8 group.

Table 3. Relevant character tables of the PI groups listed in figure 4.
(*a*) G_4 group with the inversion operator.

G_4	E	(12)	E*	(12)*
A^+	1	1	1	1
B^+	1	−1	1	−1
A^-	1	1	−1	−1
B^-	1	−1	−1	1

(*b*) G_8 group for 'flipping + donor tunnelling' being feasible.

G_8	E	(12)	(34)	(12)(34)	E*	(12)*	(34)*	(12)(34)*
A_a^+	1	1	1	1	1	1	1	1
A_b^+	1	1	−1	−1	1	1	−1	−1
B_a^+	1	−1	1	−1	1	−1	1	−1
B_b^+	1	−1	−1	1	1	−1	−1	1
A_a^-	1	1	1	1	−1	−1	−1	−1
A_b^-	1	1	−1	−1	−1	−1	1	1
B_a^-	1	−1	1	−1	−1	1	−1	1
B_b^-	1	−1	−1	1	−1	1	1	−1

(*c*) C_2 group for a single donor tunnelling.

C_2	E	(12) or (12)*
A	1	1
B	1	−1

(*d*) Pure permutation group G4 for only the donor tunnelling being feasible in the trimer-d_5 and -d_1.

G_4	E	(12)	(34)	(12)(34)
A_a	1	1	1	1
A_b	1	1	−1	−1
B_a	1	−1	1	−1
B_b	1	−1	−1	1

The symmetry species of the tunnelling state can be any one of the eight irreps. Because of the operators P* (product of a permutation operation P and the inversion E*), the complete internal wavefunction can have two different irreps in G_8, namely, $A_a^{\pm}$ for the trimer-d_5, and $B_b^{\pm}$ for the trimer-d_1. The character tables of G_4 [with (12)* as the generator] and G_8 are given in table 3(*a*, *b*).

The symmetry of the overall rotational wavefunction can be classified by examining the equivalent rotations of the PI operators. Equivalent rotations should be determined in a consistent reference coordinate system. A right-handed molecule fixed axis system *xyz* is defined to be coincident with the principal axis system *abc* with the following assignment $x \leftrightarrow a$, $y \leftrightarrow b$, and $z \leftrightarrow c$. Unlike the pure trimer, wherein a single

flip causes the *a* and *b* inertia axes to rotate by 120°, the trimer-d_5 or -d_1 always has its *b* or *a* axis, respectively, passing through the unique HOD monomer. The directions of the trimer-d_5 *xyz* system are defined such that the *y* coordinate of the oxygen in the unique HOD is always positive, the *x* coordinate of O_b (figure 1) is always positive, and the unit vector of the *z* axis follows the right handed rule: $\mathbf{z} = \mathbf{x} \times \mathbf{y}$. With the above definition, the pure permutation operators (P) in G_8 are equivalent to no rotation at all (R_0), while the P* operators correspond to a rotation of π about the *z* axis (R_z^π). The effect of the equivalent rotations R_0 and R_z^π on the Euler angles $\Omega = (\theta, \phi, \gamma)$ and the overall rotational basis wavefunction $|J, k, m\rangle$ [63] ($k = |K|$) is

$$R_z^\pi(\theta, \phi, \gamma) = (\theta, \phi, \gamma + \pi), \tag{2}$$

$$R_z^\pi |J, k, m\rangle = (-1)^k |J, k, m\rangle. \tag{3}$$

Consequently, the final Wang-symmetrized rotational wavefunction transforms as A_a^+ for k = even, and A_a^- for k = odd, wherein A and the subscript 'a' correspond to the +1 character under (12) and (34), respectively.

A VRT correlation diagram (figure 4(*c*)) can be generated based on the G_8 group and the above analysis. Flipping generates a manifold of pseudorotational states labelled by $A^\pm$ irreps classified under the C_s group. The pattern of the torsional levels depends on the specific arrangement of the mixed trimer (see the discussion in section 6); for the mixed trimers with all three free flipping atoms being of the same isotope, say H, the torsional levels are similar to the pseudorotational manifold of the corresponding homogeneous trimer, $(H_2O)_3$ accordingly (figure 4(*a*)). The donor

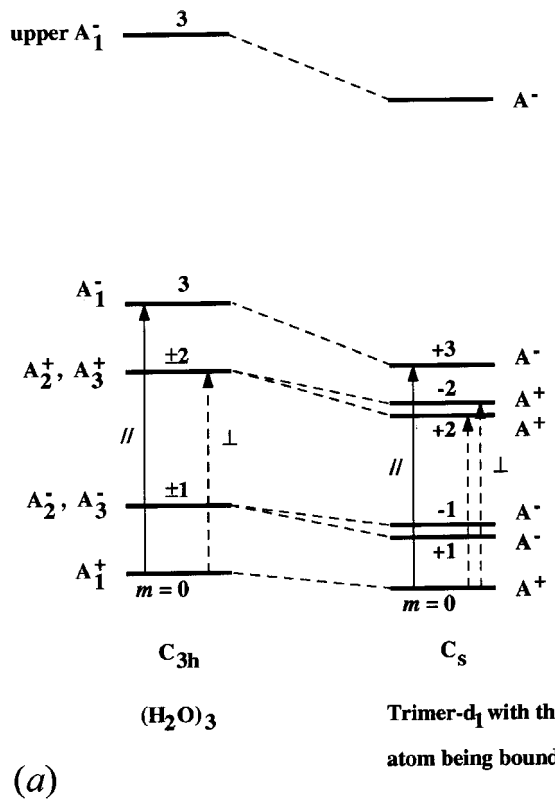

Figure 4. For legend see facing page.

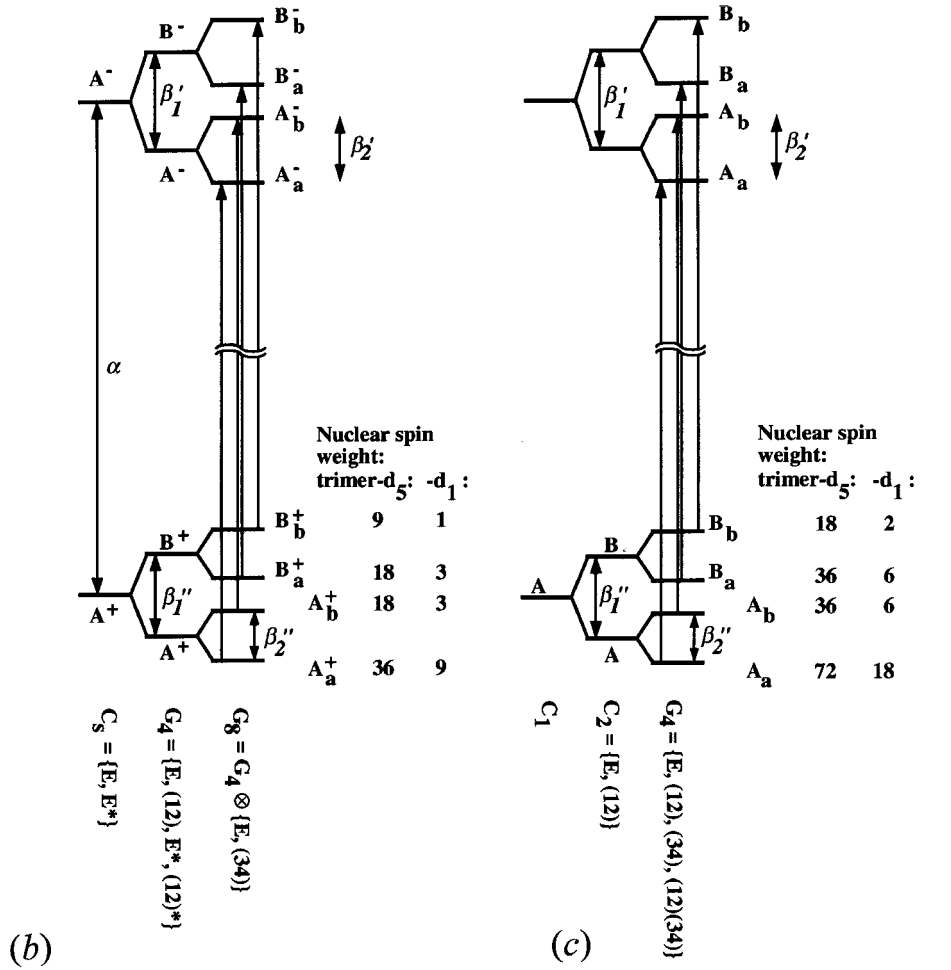

Figure 4. Schematic correlation diagrams used to interpret the observed VRT states for the mono- and pentadeuterated cyclic trimers. (*a*) Correlation between the pseudorotational states classified under C_s for the trimer-d_1 wherein the unique D atom is bound and under G_6 for $(H_2O)_3$. The pseudorotational manifold results from torsion of each monomer approximately about its bound O–H(D) bond, which connects 6 isoenergetic frameworks [6, 9, 30, 34]. The red shifts of the trimer-d_5 eigenstates are caused by the smaller reduced internal rotational constants. The parallel ($\parallel$) and perpendicular ($\perp$) types of transition are illustrated by the solid and dashed arrowed lines, respectively. Note that the degenerate (due to the G_6 symmetry) pseudorotational states of $(H_2O)_3$ are resolved in the trimer-d_1. Two scenarios are proposed for the observed quartet splitting: (*b*) the flipping+donor tunnelling mechanism, in which the donor tunnelling pathway most likely involves the exchange+double flip pathway (see text) and the MS group is G_8; (*c*) donor tunnelling alone mechanism, in which the motion is effectively a C_2 rotation of a monomer and the appropriate PI group G_4 is the only *pure permutation* group that can reproduce the observed pattern. The pseudorotational spacing α should be much larger than the rotational energy separations. In either case, β_1 is the tunnelling splitting caused by the exchange of the bonded and free atoms within one monomer, and β_2 for this process by the other monomer.

tunnelling superimposes a quartet of spacings β_2, $(\beta_1 - \beta_2)$, β_2, as discussed above, onto each torsional state. The G_4 group is the direct product group of C_s and the C_2 group that permits the more facile donor tunnelling. The final G_8 group is equal to $C_s \otimes C_2$ ($\{E_2(12)\} \otimes C_2$ ($\{E, (34)\}$). The correlation between C_s and G_4, G_4 and G_8 can be summarized as follows:

$$C_s \leftrightarrow G_4: \quad A^{\pm} \leftrightarrow A^{\pm} \oplus B^{\pm}, \tag{4}$$

$$C_4 \leftrightarrow G_8: \quad A^{\pm} \leftrightarrow A_a^{\pm} \oplus A_b^{\pm}$$

$$B^{\pm} \leftrightarrow B_a^{\pm} \oplus B_b^{\pm}. \tag{5}$$

Both sets of quartets resemble the observed spacing pattern.

The nuclear spin weight of each irrep Γ_{VRT} can now be calculated following the rules of multiplication between different symmetry species: $A \otimes B = B$, $A \otimes A$ or $B \otimes B = A$ (the same relations hold for the subscripts a and b), and $+ \otimes - = -$. From the spin weights (figure 4(*b*)) associated with each irrep in the correlation diagram, the observed *intensity* pattern 4:2:2:1 (predicted spin weight ratio = 36:18:18:9) is realized for the trimer-d_5, as well as for the trimer-d_1, observed to be 9:3:3:1 (prediction = 9:3:3:1).

The electric dipole selection rule is determined by satisfying $\Gamma''_{VRT} \otimes \Gamma'_{VRT} \supset \Gamma^*$, where Γ^* ($\Gamma^* = A_a^-$ in G_8) is the irrep of the dipole moment. Therefore, VRT transitions occur as

$$\Gamma_i^+ \leftrightarrow \Gamma_i^-, \tag{6}$$

where Γ = A, B and i = a, b. Accordingly, we expect a parallel band (ΔK_c = even) for the $A^+ \leftrightarrow A^-$ pseudorotational transitions and a perpendicular band (ΔK_c = odd) between states of the same pseudorotational symmetry under C_s. Thermal relaxation occurs between states of the same Γ_i symmetry regardless of the parity [59]. In a cold molecular beam (T_{rot} = 5 K), this can make the upper quartet much less populated than the lower one if α, the pseudorotational spacing is larger than kT_{rot}, where k is the Boltzmann constant.

The above quartet pattern can also be deduced with the donor tunnelling pathway alone. This would lead to a symmetry group G_4. We stress here, however, the only G_4 group (table 3(*d*)) which reproduces the correct quartet intensity pattern is the pure permutation group formed by {E, (12), (34), (12)(34)}; it requires the effective C_2 rotation as the only feasible tunnelling pathway. The other G_4 = {E, (12)*, (34)*, (12)(34)} group (table 3(*a*)) alone would produce a spin weight ratio of (36+9):(18+18):(18+18):(9+36) for the trimer-d_5, thereby excluding the 'exchange+double flip' pathway. The summation here is over the contributions to the symmetric and antisymmetric complete internal wavefunctions, which correspond to two different irreps in a PI group. In a pure permutation group, the symmetries of both internal wavefunctions correspond to the same irrep, and the two sets of spin weights are equal; the resulting ratios are (36+36):(18+18):(18+18):(9+9) for the trimer-d_5 and (9+9):(3+3):(3+3):(1+1) for the trimer-d_1 (figure 4(*c*)). The symmetry properties, e.g., the selection rules, in the pure permutation G_4 group are similar to those derived in G_8, except that the $\pm$ signs should be dropped. We note that although the C_2 tunnelling alone can account for the observed quartet feature, it is inadequate for classifying the symmetry properties such as the transition type of the observed vibration; the vibrational symmetry in the pure permutation group G_4 is always totally symmetric. Nevertheless, we do not distinguish the $\pm$ symmetry labels in the following discussion of the quartet splitting.

The observed quartet feature is not a direct measure of the absolute donor tunnelling splittings, but we can establish the relative magnitudes between the upper and lower states based on the tunnelling intensity pattern and the symmetry ordering of the ground state quartet displayed in figure 4. Since the A_a state (the lowest energy and most intense component) was observed to the red side of the quartet, we have measured only the difference between the excited and ground state tunnelling splittings; the former must be larger than the latter. Using the singly and doubly primed symbols for the ground and upper state donor tunnelling splittings, respectively, we can quantify the two slightly different donor tunnelling splittings explicitly as follows:

$$\beta'_1 - \beta''_1 = 13{\cdot}7\ \text{MHz}, \quad \beta'_2 - \beta''_2 = 10{\cdot}5\ \text{MHz for the trimer-}d_5;$$
$$\beta'_1 - \beta''_1 = 277{\cdot}5\ \text{MHz}, \quad \beta'_2 - \beta''_2 = 265{\cdot}0\ \text{MHz for the trimer-}d_1.$$

Note that it is the difference of $(\beta_1 - \beta_2)$ values, $(\beta'_1 - \beta'_2) - (\beta''_1 - \beta''_2)$, between the ground and excited states that gives the spacing of the middle doublet in all the observed mixed trimer quartets (3·2 MHz for the trimer-d_5, 12·5 MHz for the trimer-d_1). If $(\beta_1 - \beta_2)$ is itself within the spectral resolution, inasmuch as the A_b and B_a states are then practically accidentally degenerate, one would see a triplet with the intensity of the middle component simply proportional to the sum of the spin weights of the normal middle doublet, which may be the origin of the trimer-d_5 $K_c = 0$ triplet. This implies a coupling between the tunnelling motion and the overall rotation along the symmetry axis, thereby producing a *K*-dependent tunnelling splitting [7].

Close magnitudes of the tunnelling splittings between the homogeneous and mixed isotopomers, 5 MHz for $(D_2O)_3$ [6, 9–11] versus 10·5 MHz for the trimer-d_5, 289·4 MHz for $(H_2O)_3$ [9] versus 265 MHz in the trimer-d_1, suggest that a similar type of tunnelling motion is operative, while their finite differences imply that the same type of tunnelling in different isotopomers samples slightly different regions of the potential surface. Hence, measurements of the tunnelling splittings in a series of isotopic trimers [64] could provide a sensitive test of a model IPS.

Finally, we point out that other possible trimer isotopomers should not produce the observed quartet if there are fewer than two identical homogeneous monomers. Among those are $(HOD)_2D_2O$ and $(HOD)_2H_2O$ with various arrangements of H or D in bound or free positions. Considering both simultaneous flipping and donor tunnelling or, alternatively, only the donor tunnelling as the feasible motions would lead to a doublet of 2:1 and 3:1 intensity ratios for the single D_2O and the single H_2O trimers, respectively. Again, only the pure permutation C_2 group produces these spin weight ratios when the simultaneous flipping motion becomes infeasible. In a trimer that has three pure monomers of different kinds, e.g., $(D_2O)_2H_2O$, the correlation diagram can be constructed by employing the donor tunnelling pathways with splittings of appropriate magnitudes: namely, the splitting for H_2O should be generally larger than for D_2O. Hence, a pure permutation group $G_8 = C_2 \otimes C_2 \otimes C_2$ is sufficient to predict the tunnelling splitting pattern for $(D_2O)_2H_2O$ as two sets of widely separated quartets (caused by the H_2O exchange tunnelling) of a 6:2 intensity ratio between them, and 72:36:36:18 within them. The absence of all these possible tunnelling fine structure features further supports our assignment of the two observed bands to the trimer-d_5 and -d_1.

5. Structure determination

In non-rigid molecular systems possessing large amplitude motions (LAMs), extracting accurate equilibrium structural parameters from the measured vibrationally averaged spectroscopic properties has traditionally been a difficult task [65]. Even with the well documented vibrational averaging corrections, conventional isotope substitution methods for structure determination apply only to semi-rigid systems in which possible LAMs either occur on a time scale much slower than the overall rotational period (as in the umbrella inversion of NH_3) or not at all. For systems with extensive LAMs, as in the torsional modes of the water trimer in which the 3-dimensional zero-point energy (ZPE) is above the potential barrier [39] and the notion of tunnelling itself becomes irrelevant, structural parameters obtained on a basis of a nearly rigid geometry [4–6] are not reliable. Although the experimental vibrationally averaged structure can be used to characterize general aspects of the IPS (e.g., oblate symmetric top spectrum confirms the ring structure of the trimer), the ability to reliably extract specific structural information (e.g., the O—O separation in water clusters), in turn, relies ultimately on a knowledge of the nuclear wavefunctions on the multidimensional potential surface.

Arguably, the advent of modern computational techniques has made the simulation of the quantum mechanical averaging dynamics the most plausible way to connect a high-dimensional IPS with the vibrationally averaged rotational constants determined by experiment [41]. Such complex averaging dynamics in the pure water trimer have been unambiguously manifested in the observed [9] rigorously *symmetric* oblate top structure ($\kappa = 1$) as a result of the free proton flipping motions, whereas the calculated equilibrium geometry is *asymmetric*. Our previous trimer structure models [4–6] either neglected this dynamic symmetry, as in the model based on the rigid asymmetric equilibrium geometry, or were unable to reproduce the observed large negative zero point inertial defect (non-planarity), as in the point-mass model. In the following structure simulations, we address both principal experimental features using an ensemble average of the inverse inertia tensors sampled according to a probability distribution function of the flipping angle.

Quantum mechanically, the measured rotational constants are averaged as $\langle \text{vib.}|\mathbf{B}|\text{vib.}\rangle$ [66], where $|\text{vib.}\rangle$ is the vibrational wavefunction and $\mathbf{B}$ is inversely proportional to the instantaneous inertia tensor ($\mathbf{I}$), which is, in turn, a function of all the intra- and intermolecular coordinates. In this work, only averaging over the flipping vibrational wavefunction was considered, while the structural parameters in other degrees of freedom were either fixed or systematically varied to best reproduce the observed rotational constants; specifically, the root-mean-square (rms) of $(B_{\text{obs.}} - B_{\text{calc.}})$ was minimized in this procedure.

It is the average of the inverse inertia tensor, $\langle \mathbf{I}^{-1} \rangle$ and *not* $\langle \mathbf{I} \rangle^{-1}$, that is actually determined in the VRT experiments and which we calculate in the simulation. Furthermore, the measured rotational constants should be simulated as the averaged value of a function, $\langle \mathbf{I}^{-1} \rangle$, not a function of averaged variables, $\mathbf{I}^{-1}[\langle R(\text{O—O}) \rangle, \langle \omega \rangle$, etc.], where ω represents the flipping angles (figure 1); the difference between these averages is small only when there is no LAM. For the single flipping coordinate, the latter approach poses a problem since there are enantiomeric potential wells corresponding to the preferred positions of a free proton above and below the O···O···O plane. The averaged proton position is in the plane, which leads to a planar trimer structure with zero or positive zero point inertial defect, in contrast to the

observed large negative value [67]. A second problem of the latter approach is that the free protons appear to be further away from the symmetry axis, and as a consequence $\langle R(\mathrm{O—O})\rangle$ would artificially contract in order to reproduce the measured $\langle \mathbf{B}\rangle$.

The integral $\langle \omega|\mathbf{B}|\omega\rangle$ was evaluated using the Monte Carlo (MC) technique. The one-dimensional vibrational ground state wavefunction $|\omega_a|$ has been calculated by Gregory and Clary in their DQMC studies of the three-body effect in the water trimer [41]. A probability distribution function (pdf), $\langle \omega_a|\omega_a\rangle$, was simulated by two Gaussian functions constructed to be symmetric relative to the O···O···O plane with the same standard deviation (SD) (figure 5). The pdf was sampled with the conventional rejection algorithm, generating a typical set of about 2×10^5 flipping angles for each ω. For each instantaneous structure, which corresponds to a *random* combination of $\{\omega_a, \omega_b, \omega_c\}$, the inverse inertia tensor was calculated with respect to a reference coordinate system. Then the entire ensemble of the inverse inertia tensors was averaged in the *same* axis system, and finally diagonalized to produce the calculated average rotational constants, which can be compared directly with the experimental values.

Special attention is paid to the combination of $\{\omega_a,\omega_b, \omega_c\}$. Since the instantaneous ground state structure corresponds to a correlated arrangement with two free protons above and one below the O···O···O plane, we have excluded the choice of all three angles having the same sign corresponding to the 'uuu' or 'ddd' crown structures. In a case study of the uncorrelated random combination of all three angles, it was found that the crown structures constitute only a miniscule fraction of the overall samples. Excluding them from the sample set caused a $< 0{\cdot}04\%$ decrease in $\langle R(\mathrm{O—O})\rangle$. A detailed knowledge of the correlation among $\{\omega_a, \omega_b, \omega_c\}$ other than the crown structure is beyond the accuracy needs of the present model and therefore has not been considered.

By simulating the flipping motions in this manner, we reproduce the two salient structural features observed for the homogeneous trimers which possess C_{3h} ($= C_3 \otimes C_s$) dynamic symmetry. When a sufficient number of structures are averaged, the off-diagonal matrix elements $\langle \mathbf{I}^{-1}\rangle_{xz}$ and $\langle \mathbf{I}^{-1}\rangle_{yz}$ (z being an odd function of ω) approach zero (E* symmetry). This partitions the matrix into 2×2 and 1×1 diagonal subblocks. The diagonal elements $\langle \mathbf{I}^{-1}\rangle_{xx}$ and $\langle \mathbf{I}^{-1}\rangle_{yy}$ becomes equal (C_3 symmetry): This is the origin of the exact symmetric top behaviour observed in the VRT spectra. And $\langle \mathbf{I}^{-1}\rangle_{xx}$ is not equal to $\langle \mathbf{I}^{-1}\rangle_{zz}/2$ because the $\langle mz^2\rangle$ terms (with implied summation over all the atoms) constitute an even function of ω and cannot be averaged to zero by the out-of-plane flipping motions; this gives rise to the observed negative zero-point inertial defect.

The monomer geometry in the trimer, taken from the MP2 level calculations by Schütz *et al.* [34] (choice of the other similar *ab initio* values [25, 29] introduces only $\ll 1\%$ deviations from the intermolecular parameters reported below), was fixed in all the simulations. The bond length of the free O—H(D) bond was 0·959 Å, while the bound O—H(D) exhibited an elongated length of 0·971 Å. The monomer bond angle was fixed at 103·95°. Furthermore, all the bound H or D atoms were fixed in the O—O—O plane, although they are slightly out of plane in the equilibrium structures. Other constraints (figure 1) included: (i) the three R(O—O)s were equal for all the trimers; (ii) $\phi_a = \phi_b = \phi_c$ for the pure trimers, but were independently varied for the trimer-d_5; (iii) the most probable flipping angle, ω_{prob}, was set equal for each monomer, and the SD of each Gaussian was fixed at 19·5° according to our simulation which reproduced the DQMC wavefunction.

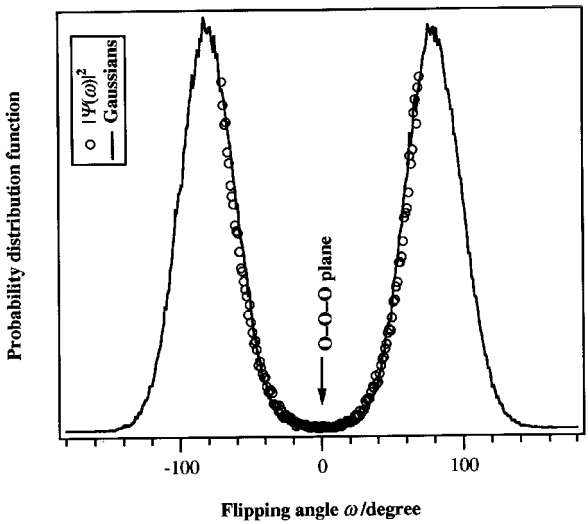

Figure 5. The pdf for the out-of-plane flipping angle ω defined in figure 1. The circles are the squared one-dimensional wavefunction of ω reported by Gregory and Clary [41] which, in turn, is simulated by two Gaussians of equal SDs. Both the reproduced wavefunction and the Gaussian pdf were sampled using a rejection algorithm. The flipping angles obtained by sampling the Gaussian pdf were then used in the averaged inverse inertia tensor calculation.

Table 4. Average structural parameters obtained from the MC simulation of the trimer flipping dynamics. The experimental values (whenever available) are listed in parentheses for comparison. The root-mean-square errors of all the simulations are < 1 MHz; the exact values depend on the number of samples averaged in the simulation. See text for the extraction of an averaged structure. The band origins are given in parentheses next to each spectral carrier.

	$(H_2O)_3$ (87·1 cm^{-1})	$(D_2O)_3$ (98·1 cm^{-1})	trimer-d_5 (97·26 cm^{-1})
A''/MHz	6647·10	5796·24	6195·93
	(6646·94)	(5796·19)	(6195·69)
B''/MHz	6646·60	5795·68	5833·31
	(6646·94)	(5796·19)	(5833·90)
C''/MHz	3389·31	2999·41	3094·93
	(—)	(3088·46)[a]	(—)
Δ_0/amu Å^2	− 2·956	− 5·898	− 4·91
	(—)	(− 10·75)[a]	(—)
κ	0·9997	0·9996	0·766
	(+1)	(+1)	(—)
R_0(O—O)/Å	2·840	2·837	2·846
ϕ_a/deg[b]	21·0	21·0	24·6
ϕ_b/deg[b]	21·0	21·0	11·0
ϕ_c/deg[b]	21·0	21·0	15·0
$\lvert\omega_{prob}\rvert$/deg[c]	50·0	50·0	50·0
SD of $\lvert\omega_{prob}\rvert$/deg	19·5	19·5	19·5

[a] The difference here is due mainly to the non-structural Coriolis contamination.
[b] Refer to figure 1 for the specific angle definitions.
[c] $\omega = 0$ corresponds to the flipping bond lying in the O—O—O plane.

A typical set of simulated rotational constants is summarized in table 4 together with the average structural parameters for $(H_2O)_3$, $(D_2O)_3$, and the trimer-d_5. Since a range of R(O—O), ϕ, and ω_{prob} can yield the same quality (< MHz rms) results (figure 6), a particular set of structural parameters that produced the calculated constants is not as interesting as the set of the averaged values [R_0(O—O), ϕ_0, and $\omega_{0,prob}$], which should be interpreted cautiously as being correlated because they outnumbered the experimental rotational constants. Note that the average R(O–O) distances are about 0·04 ~ 0·05 Å smaller than all previous experimentally deduced values [4, 5].

The dependence of R(O—O) on ϕ and ω_{prob} for $(H_2O)_3$ and $(D_2O)_3$ are given in figure 6(a, b), in which all the data points represent an optimized structure which

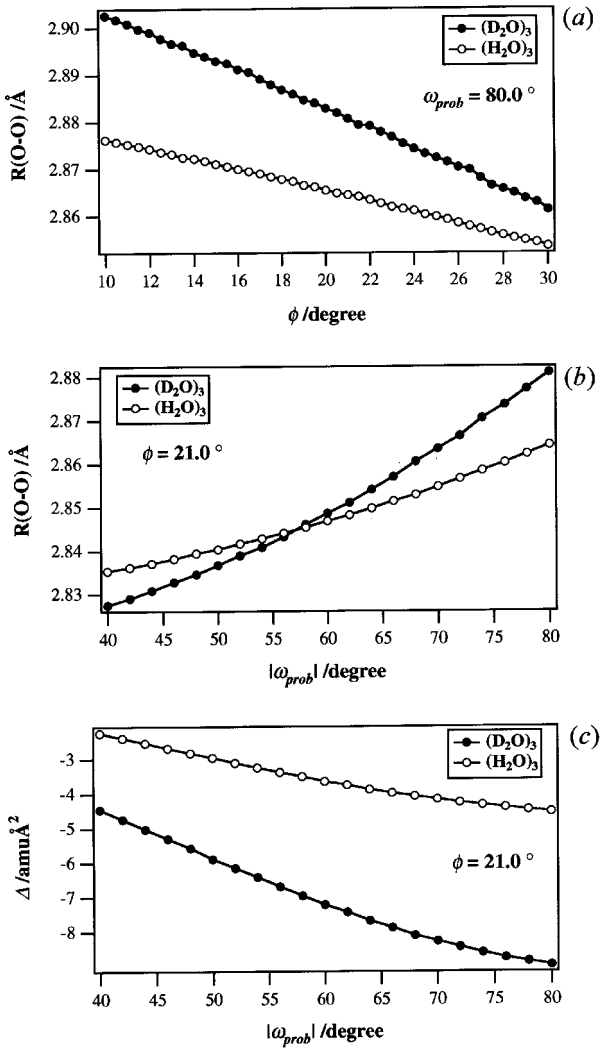

Figure 6. Observed correlations among the intermolecular coordinates and the inertial defect in the MC structural simulations of $(H_2O)_3$ and $(D_2O)_3$. Each data point represents an optimized trimer structure that reproduced experimental $A'' = B''$ constants with 1 MHz rms, averaging over ~ 2×10^5 instantaneous flipping geometries. The averaged R(O—O) was obtained with ω_{prob} and ϕ fixed close to their respective equilibrium values, 50·0° and 21·0°.

reproduces the observed rotational constants with an rms less than the experimental uncertainty (< 1 MHz). It was found in most high level *ab initio* calculations that the equilibrium ϕ_e is $20 \sim 21°$, and R_e(O—O) is $\sim 2{\cdot}80$ Å. If R(O—O) is expanded in the neighbourhood of the averaged geometry for the pure trimers as

$$R(\text{O—O}) = R_0(\text{O—O}) + \left(\frac{\partial R}{\partial \phi}\right)\Bigg|_{\phi=\phi_0} (\phi - \phi_0) + \left(\frac{\partial R}{\partial |\omega_{\text{prob}}|}\right)\Bigg|_{|\omega_{\text{prob}}|=|\omega_{0,\text{prob}}|} (|\omega_{\text{prob}}| - |\omega_{0,\text{prob}}|) + \text{high order terms}, \quad (7)$$

we see from figure 6(a, b) that $\partial R/\partial\phi < 0$ and $\partial R/\partial|\omega_{\text{prob}}| > 0$, and the high order terms in ω, are more important than in ϕ. If we choose $\phi_0 = 21{\cdot}0°$ and $\omega_{0,\text{prob}} = 50{\cdot}0°$ [36, 37], which are close to their corresponding equilibrium values, then the average R_0(O—O) for $(H_2O)_3$ is found to be 2·840 Å, and only slightly smaller (2·837 Å) for $(D_2O)_3$. Considering that $(D_2O)_3$ has a lower ZPE than $(H_2O)_3$, this result seems reasonable. However, with the above ϕ_0 and $\omega_{0,\text{prob}}$, the calculated Δ_0 (figure 6(c)) was only $-5{\cdot}90$ amu Å^2 compared with the measured $-10{\cdot}75$ amu Å^2 for $(D_2O)_3$ [9]. Since the out-of-plane motion contributes negatively to Δ_0 while the in-plane motion contributes positively, this suggests either that the simulation of other out-of-plane motions, e.g., from the bound atoms which were constrained to be in the O—O—O plane, is insufficient, or that the measured Δ_0 has non-structural contributions, e.g., the Coriolis coupling between the pseudorotation and the overall vibration along the c axis, which was not incorporated explicitly in the fitting Hamiltonian and thus gave a contaminated non-structural C constant. Evidence of this Coriolis coupling was found in the perturbation of the $K = 1 \leftarrow 0$ subband and the abnormal quartet appearance of the $K = 0 \leftarrow 1$ subband for the 98·1 cm^{-1} $(D_2O)_3$ band, which has not been elaborated in our previous work [9]. For this reason, the C constant was not considered in the rms minimization.

For the trimer-d_5, a combination of $\{\phi_a, \phi_b, \phi_c\} = \{351{\cdot}1 \pm 1{\cdot}0°,\ 11{\cdot}0 \pm 1{\cdot}0°,\ 15{\cdot}0 \pm 1{\cdot}0°\}$ reproduced the measured A and B constants with an rms of less than 1 MHz at a most probable flipping angle of $|\omega_{\text{prob}}| = 80{\cdot}0°$, a value chosen according to the DQMC wavefunction. The resulting R(O—O) was $2{\cdot}872 \pm 0{\cdot}001$ Å. The difference among $\{\phi_a, \phi_b, \phi_c\}$ can be rationalized in terms of the nature of the D bond: while ϕ_a represents the nonlinearity of an O—D$\cdots$(OHD) bond, both ϕ_b and ϕ_c characterize a similar kind of bond, O—D$\cdots$(OD$_2$); the difference between ϕ_b and ϕ_c is thus much smaller than that between ϕ_a and $\{\phi_b, \phi_c\}$. Interestingly, the average of the $\{\phi_a, \phi_b, \phi_c\}$ angles is near the equilibrium values, $20 \sim 21°$. The difference in $\{\phi_a, \phi_b, \phi_c\}$ for the trimer-d_5 largely supports the essential concept underlying our tunnelling fine structure analysis, namely, the two D$_2$O monomers are not chemically equivalent, which is the origin of the two slightly different donor tunnelling splittings, and hence the observed quartet (rather than triplet) feature. A simulation of the trimer-d_5 with the unique H atom in the bound position has also been tested, but the measured rotational constant could not be reproduced satisfactorily without the rms being larger than 40 MHz, which is a strong basis for assigning the H atom as being in the free position. Again, strong correlations between all the structural parameters should be expected, even though the dependence of R(O—O) on $|\omega_{\text{prob}}|$ and the angles ϕ has not been examined extensively. But the same positive $\partial R/\partial|\omega_{\text{prob}}|$ behaviour [R(O—O) contracts as the flipping H and D atoms get closer (smaller $|\omega_{\text{prob}}|$) to the O—O—O

plane] was observed at a few $|\omega_{\text{prob}}|$ angles. To be consistent with the homogeneous trimer simulations, the optimal (rms < 1 MHz) R_0(O—O) was found to be $2{\cdot}846 \pm 0{\cdot}003$ Å with fixing $|\omega_{0,\text{prob}}| = 50{\cdot}0°$ and varying $\{\phi_a, \phi_b, \phi_c\} = \{24{\cdot}6 \pm 3{\cdot}5°, 11{\cdot}0 \pm 3{\cdot}0°, 15{\cdot}0 \pm 1{\cdot}0°\}$.

6. Vibrational analysis

The intermolecular vibration dynamics of $(H_2O)_3$ and $(D_2O)_3$ have been investigated extensively by Schütz *et al.* (1-dimensional model) [34], Klopper and Schütz (2-dimensional model) [38], and Sabo *et al.* (3-dimensional calculation including all three ω coordinates) [39] in a series of theoretical studies addressing the torsional subspace (the flipping motions of the free O—H(D) bonds) on a modified empirical IPS [36, 37]. All the observed pure trimer bands have been assigned to the pseudorotational states which can be classified under the C_{3h} MS group generated by the flipping motions, although the agreement is not very satisfying.

Neglecting the Coriolis coupling between the overall rotation and the flipping motion and coupling between flipping and other vibrational motions, we can write the effective 3-dimensional Hamiltonian [38, 39, 61] for the hydrogen bond torsion as follows:

$$H_{\text{tor}} = -\sum_{i=a,\,b,\,c} F_i \frac{\partial^2}{\partial \omega_i^2} + V(\omega_a, \omega_b, \omega_c), \tag{8}$$

where F_i are the reduced internal constants for the three flipping O—H(D) bonds and $V(\omega_a, \omega_b, \omega_c)$ is the effective torsional potential, which to a good approximation possesses the G_6 symmetry for all the trimer isotopomers. For $(H_2O)_3$, $(D_2O)_3$ and $(HOD)_3$ with all the H or D atoms being free, all three F_i constants are, on the average, identical, thereby allowing the pseudorotational states to be classified under G_6.

Based on equation (8), isotope substitutions (only the hydrogens) in the homogeneous trimers principally cause two effects; both concern the change in the kinetic energy. First, the F_i constants are no longer equivalent due to the asymmetric (vibrationally averaged) distribution of the atom masses; in the case in which all the flipping atoms are of the same isotope, the differences between F's are small but non-negligible. Thus the pseudorotational states can be classified properly only under the group C_s. Second, the pseudorotational energies shall be modified; this would translate into a slight shift of the vibrational band origin when the change in F_i is small, which corresponds to isotope substitutions in the bound positions.

We therefore assign the trimer-d_1 band observed at ~ 86 cm^{-1} to the same pseudorotational transition, A_1^- ($m = 3$) $\leftarrow A_1^+$ ($m = 0$), as the $(H_2O)_3$ band at $87{\cdot}1$ cm^{-1}; only the pseudorotational symmetries need to be adapted to $A^- \leftarrow A^+$. The unique D atom must be in the D bonded position, even though a simulation of the rotational constants is not available. The reduced internal rotational constants of the trimer-d_1 are, on the average, smaller than those of $(H_2O)_3$. A 1-dimensional pseudorotation model calculation similar to that of Schütz *et al.* [34] predicts that a $0{\cdot}1$ cm^{-1} decrease in the average F_i can cause a $0{\cdot}77$ cm^{-1} red shift (from $91{\cdot}05$ to $90{\cdot}28$ cm^{-1} at a barrier height of 480 cm^{-1}) of the band origin for the A_1^- ($m = 3$) $\leftarrow A_1^+$ ($m = 0$) transition of $(H_2O)_3$; the average F_i of $(H_2O)_3$ was calculated to be $20{\cdot}26$ cm^{-1}. Calculation of the reduced rotational constants based on rigid trimer structures produced only a $0{\cdot}003$ cm^{-1} decrease for the trimer-d_1, which would suggest a much smaller red shift than the observed $1{\cdot}1$ cm^{-1} value. To improve the discrepancy, one needs to consider two factors. First, evaluation of the F_i constants requires a knowledge of the torsional pathway and the proper inclusion of the vibrational

averaging effect; all three bound H(D) atoms in the slightly puckered trimer ring are coupled to move upon a single flip, as required by the G_6 symmetry of the torsional potential. Second, the differences between three F_i constants should be treated properly in calculating the pseudorotational states; a 1-dimensional model is not suited to consider these differences.

The 97·26 cm^{-1} trimer-d_5 band, however, deviates dramatically from the pseudorotational states described by C_{3h} because the unique H atom is free. Detailed calculations using a 3-dimensional discrete variable representation (DVR) scheme similar to the one by Sabo *et al.* clearly are needed for the various mixed trimers. If the observed new band corresponded to the same type of pseudorotational transition in $(D_2O)_3$, the closest possible transition of the same parallel type would be the 89·6 cm^{-1} hot band. But, arguing against this it was found that the trimer-d_5 signal decreased with increasing temperature of the sample. Furthermore, the 6·7 cm^{-1} blue shift here should be comparable with the amount of the red shift ($\sim$ 1·1 cm^{-1}) found for the trimer-d_1 if H occurred in the bonded positions. The next possible close lying pseudorotational transition in $(D_2O)_3$ which may be correlated to this observed parallel band is the A_1^- (m = upper 3) $\leftarrow A_1^+$ (m = 0) transition, which is predicted to be 96·15 cm^{-1} or 88·93 cm^{-1} depending on the choice of 3-dimensional torsional potentials [61, 62]. In the trimer-d_5, since one of the three flipping masses is the light H, this band is expected to be blue shifted. Based on the selection rules under C_s, it is most likely that the 97·26 cm^{-1} parallel band of trimer-d_5 corresponds to the A^- (m = upper 3) $\leftarrow A^+$ (m = 0) pseudorotational transition.

The low frequency band origin and the consistently slightly smaller A' and B' constants compared with A'' and B'' lead us to attribute the 97·26 cm^{-1} vibration to the out-of-plane torsion about the D bonds. The lack of an effective C_{3h} dynamic symmetry is responsible for the asymmetric top behaviour. If the pseudorotation primarily excited the torsional coordinates ω, simulations of the excited state constants with other coordinates (R(O—O) and ϕ) fixed to their ground state values, in principle, would tell us the change in ω_{prob} and its SD. Our study showed that either $|\omega_{prob}|$ decreases or SD increases in the excited state; both are consistent with having a more delocalized torsional wavefunction upon vibrational excitation [36].

7. Conclusion

Spectroscopic measurements of the intermolecular vibrational bands and tunnelling splittings of the mixed trimer isotopomers have revealed modified HBNR dynamics from those found in $(H_2O)_3$ and $(D_2O)_3$. The simplified molecular symmetry effected by isotopic substitution has varied the energy levels corresponding to the flipping and donor tunnelling (bifurcation) motions. Two rearrangement scenarios have been proposed to interpret the quartet or triplet VRT patterns observed in the trimer-d_5 and -d_1: The first involves both the flipping and bifurcation pathways, whereas the second employs only a bifurcation mechanism which is an effective C_2 rotation of a monomer unit. In either case, it is the exchange of the bound and free D or H within two slightly different D_2O or H_2O monomer units, respectively, that gives rise to the tunnelling fine structure. To account fully for the symmetry properties of the observed VRT states (especially the pseudorotational manifold caused by the 3-dimensional torsional motions), however, the former is more appropriate. Therefore, the MS symmetry group for the two trimer isotopomers is G_8. Combined with the VRT data on the homogeneous trimers, the mixed trimer measurements should serve

to produce an enhanced understanding of the molecular interactions in water, particularly the non-additive three-body forces [68].

We have demonstrated that MC simulation of the LAM (specifically the flipping motions) can reproduce the two essential features observed in the VRT spectra of $(H_2O)_3$ and $(D_2O)_3$: the exact oblate symmetric top behaviour of the vibrationally averaged structure and the large negative inertial defect caused by the static and dynamic non-planarity. The resulting vibrationally averaged structural parameters were evaluated for a series of trimer species. The particularly interesting parameter R(O–O) for $(H_2O)_3$, $(D_2O)_3$, and the trimer-d_5 has been determined to be $2{\cdot}84 \pm 0{\cdot}01$ Å, which should be regarded as being somewhat correlated with other intra- and intermolecular coordinates.

The two bands observed in this work can be assigned to the pseudorotational manifold which correlates to that found in the pure trimers. The 86 cm^{-1} trimer-d_1 band is assigned to the A^- (m = 3) $\leftarrow A^+$ (m = 0) pseudorotational transition, whereas the 97·26 cm^{-1} band of the trimer-d_5 with the unique H being free can be convincingly attributed to the A^- (m = upper 3) $\leftarrow A^+$ (m = 0) transition based on the numerical results on $(D_2O)_3$ and a selection rule argument.

This work was supported by the Experimental Physical Chemistry Program of the National Science Foundation (Grant #CHE-9424482). M.R.V. thanks the Royal Commission for the Exhibition of 1851 for a postdoctoral research fellowship.

References

[1] Fraser, G. T., 1991, *Int. Rev. phys. Chem.*, **10**, 189.
[2] Saykally, R. J., and Blake, G. A., 1993, *Science*, **259**, 1570.
[3] Liu, K., Cruzan, J. D., and Saykally, R. J., 1996, *Science*, **271**, 929.
[4] Cruzan, J. D., Braly, L. B., Liu, K., Brown, M. G., Loeser, J. G., and Saykally, R. J., 1996, *Science*, **271**, 59.
[5] Liu, K., Brown, M. G., Cruzan, J. D., and Saykally, R. J., 1996, *Science*, **271**, 62.
[6] Pugliano, N., and Saykally, R. J., 1992, *Science*, **257**, 1937.
[7] Pugliano, N., Cruzan, J. D., Loeser, J. G., and Saykally, R. J., 1993, *J. chem. Phys.*, **98**, 6600.
[8] Pribble, R. N., and Zwier, Z. S., 1994, *Science*, **265**, 75.
[9] Liu, K., Loeser, J. G., Elrod, M. J., Host, B. C., Rzepiela, J. A., Pugliano, N., and Saykally, R. J., 1994, *J. Amer. chem. Soc.*, **116**, 3507.
[10] Liu, K., Elrod, M. J., Loeser, J. G., Cruzan, J. D., Pugliano, N., Brown, M. G., Rzepiela, J., and Saykally, R. J., 1994, *Faraday Discuss. chem. Soc.*, **97**, 35.
[11] Suzuki, S., and Blake, G. A., 1994, *Chem. Phys. Lett.*, **229**, 499.
[12] Huisken, F., Kaloudis, M., Kulcke, A., and Voelkel, D., 1995, *Infrared Phys. Technol.*, **36**, 171.
[13] Kim, K. S., Dupuis, M., Lie, G. C., and Clementi, E., 1986, *Chem. Phys. Lett.*, **131**, 451.
[14] Moore-Plummer, P. L., 1990, *J. molec. Struct.*, **237**, 47.
[15] Coudert, L. H., and Hougen, J. T., 1990. *J. molec. Spectrosc.*, **139**, 259.
[16] Wei, S., Shi, Z., and Castleman, A. W., 1991, *J. chem. Phys.*, **94**, 3268.
[17] Mhin, B. J., Kim, H. S., Yoon, C. W., and Kim, K. S., 1991, *Chem. Phys. Lett.*, **176**, 41.
[18] Pillardy, J., Olszewski, K. A., and Piela, L., 1992, *J. molec. Struct.*, **270**, 277.
[19] Knochenmuss, R., and Leutwyler, S., 1992, *J. chem. Phys.*, **96**, 5233.
[20] Bosma, W. B., Fried, L. E., and Mukamel, S., 1993, *J. chem. Phys.*, **98**, 4413.
[21] Burke, L. A., Jensen, J. O., Jensen, J. L., and Krishnan, P. N., 1993, *Chem. Phys. Lett.*, **206**, 293.
[22] Althorpe, S. C., and Clary, D. C., 1994, *J. chem. Phys.*, **101**, 3603.
[23] Althorpe, S. C., and Clary, D. C., 1995, *J. chem. Phys.*, **102**, 4390.
[24] Chalasinski, G., Szczesniak, M. M., Cieplak, P., and Scheiner, S., 1991, *J. chem. Phys.*, **94**, 2873.

[25] Mó, O., Yáñez, M., and Elguero, J., 1992, *J. chem. Phys.*, **97**, 6628.
[26] Xantheas, S. S., 1995, *J. chem. Phys.*, **102**, 4505.
[27] Xantheas, S. S., 1994, *J. chem. Phys.*, **100**, 7523.
[28] Xantheas, S. S., and Dunning, Jr., T. H., 1993, *J. chem. Phys.*, **98**, 8037.
[29] Xantheas, S. S., and Dunning, Jr., T. H., 1993, *J. chem. Phys.*, **99**, 8774.
[30] Wales, D. J., 1993, *J. Amer. chem. Soc.*, **115**, 11180.
[31] Walsh, T. R., and Wales, D. J., unpublished.
[32] Fowler, J. E., and Schaefer, H. F. III, 1994, *J. Amer. chem. Soc.*, **117**, 446.
[33] van Duijneveldt-van de Rijdt, J. G. C. M., and van Duijneveldt, F. B., 1993, *Chem. Phys.*, **175**, 271.
[34] Schütz, M., Bürgi, T., Leutwyler, S., and Bürgi, H. B., 1993, *J. chem. Phys.*, **99**, 5228.
[35] Schütz, M., Bürgi, T., Leutwyler, S., and Bürgi, H. B., 1994, *J. chem. Phys.*, **100**, 1780.
[36] Bürgi, T., Graf, S., Leutwyler, S., and Klopper, W., 1995, *J. chem. Phys.*, **103**, 1077.
[37] Klopper, W., Schütz, M., Lüthi, H.-P., and Leutwyler, S., 1995, *J. chem. Phys.*, **103**, 1085.
[38] Klopper, W., and Schütz, M., 1995, *Chem. Phys. Lett.*, **237**, 536.
[39] Sabo, D., Bacic, Z., Bürgi, T., and Leutwyler, S., 1995, *Chem. Phys. Lett.*, **244**, 283.
[40] Gregory, J. K., and Clary, D. C., 1995, *J. chem. Phys.*, **102**, 7817.
[41] Gregory, J. K., and Clary, D. C., 1995, *J. chem. Phys.*, **103**, 8924.
[42] Tachikawa, M., and Iguchi, K., 1994, *J. chem. Phys.*, **101**, 3062.
[43] Rahman, A., and Stillinger, F. H., 1971, *J. chem. Phys.*, **55**, 3336.
[44] Stillinger, F. H., 1980, *Science*, **209**, 451.
[45] Reimers, J. R., Watts, R. O., and Klein, M. L., 1982, *Chem. Phys.*, **64**, 95.
[46] Jorgensen, W. L., Chandrasekhar, J., Madura, J. D., Impey, R. W., and Klein, M. L., 1983, *J. chem. Phys.*, **79**, 926.
[47] Watanabe, K., and Klein, M. L., 1989, *Chem. Phys.*, **131**, 157.
[48] Millot, C., and Stone, A. J., 1992, *Molec. Phys.*, **77**, 439.
[49] Laasonen, K., Sprik, M., Parrinello, M., and Car, R., 1993, *J. chem. Phys.*, **99**, 9081.
[50] Corongiu, G., 1992, *Int. J. Quantum Chem.*, **42**, 1353.
[51] Ohmine, I., 1995, *J. phys. Chem.*, **99**, 6767
[52] van der Avoird, A., Wormer, P. E. S., and Moszynske, R., 1994, *Chem. Rev.*, **94**, 1931.
[53] Del Bene, J. E., and Pole, J. A., 1973, *J. chem. Phys.*, **58**, 3605.
[54] Owicki, J. C., Shipman, L. L., and Scheraga, H. A., 1975, *J. phys. Chem.*, **79**, 1794.
[55] Liu, K., Brown, M. G., Carter, C., Saykally, R. J., Gregory, J. K., and Clary, D. C., 1996, *Nature*, **381**, 501.
[56] Blake, G. A., Laughlin, K. B., Cohen, R. C., Busarow, K. L., Gwo, D.-H., Schmuttenmaer, C. A., Steyert, D. W., and Saykally, R. J., 1991, *Rev. sci. Instrum.*, **62**, 1701.
[57] Liu, K., Fellers, R. S., Viant, M. R., McLaughlin, R. P., Brown, M. G., and Saykally, R. J., 1996, *Rev. sci. Instrum.*, **67**, 410.
[58] Busarow, K. L., Cohen, R. C., Blake, G. A., Laughlin, K. B., Lee, Y. T., and Saykally, R. J., 1989, *J. chem. Phys.*, **90**, 3937.
[59] Coudert, L. H., Lovas, F. J., Suenram, R. D., and Hougen, J. T., 1987, *J. chem. Phys.*, **87**, 6290.
[60] Li, J. C., and Ross, D. K., 1993, *Nature*, **365**, 327.
[61] van der Avoird, A., Olthof, E. H. T., and Wormer, P. E. S., 1996, *J. chem. Phys.*, submitted.
[62] Olthof, E. H. T., van der Avoird, A., Wormer, P. E. S., Liu, K., and Saykally, R. J., 1996, *J. chem. Phys.*, submitted.
[63] Bunker, P. R., 1979, *Molecular Symmetry and Spectroscopy* (San Diego: Academic Press) p. 235.
[64] Viant, M. R., Cruzan, J. D., Liu, K., Brown, M. G., and Saykally, R. J., 1996, to be published.
[65] Gordy, W., and Cook, R. L., 1970, *Microwave Molecular Spectra* (New York: Interscience) p. 647.
[66] Kroto, H. W., 1992, *Molecular Rotation Spectra*, 2nd Edn (New York: Dover), p. 116.
[67] Oka, T., 1995, *J. molec. Struct.*, **352–353**, 225.
[68] Elrod, M. J., and Saykally, R. J., 1994, *Chem. Rev.*, **94**, 1975.